AERODYNAMIC ANALYSIS OF FORMULA STUDENT FRONT WING USING CFD

Abbas Abasov[1], Nikoloz Kapanadze[2], Svetlana Sokolova[1]
[1]Riga Technical University, Latvia; [2]Politecnico di Torino, Italy
abbas.abasov@edu.rtu.lv

Abstract. This study presents a Computational Fluid Dynamics (CFD) investigation of an inverted multi-element front wing designed for a Formula Student racing vehicle. The wing geometry is based on the A18 aerofoil profile and incorporates a three-section mainplane with two downstream flap elements on each outboard section. Two configurations are compared: a closed-flap configuration with flap elements at 20° incidence, and an open-flap configuration with flaps normal to the mainplane chord. Two-dimensional steady-state simulations of the aerofoil cross-section were conducted in ANSYS Fluent using the SST k-ω turbulence model at 17 $m \cdot s^{-1}$, establishing baseline aerodynamic coefficients. Full three-dimensional simulations of the complete wing assembly were performed using SolidWorks Flow Simulation. The 2D analysis yields $C_L = -0.635$ and $C_D = 0.049$ for the closed configuration, and $C_L = -0.482$, $C_D = 0.019$ for the open configuration. Three-dimensional results show that opening the flap reduces downforce from 43.5 N to 28.0 N (−35.5%) and drag from 19.4 N to 10.0 N (−48.3%). Minimum pressure coefficients of $C_{p,min} \approx -3.2$ are identified at the flap leading edge in the closed configuration. Three-dimensional flow trajectory analysis reveals that the 20° closed flap generates significant upwash that impinges on the adjacent wheel – a performance-critical interaction absent in 2D analysis. The results quantify a clear aerodynamic trade-off, supporting the concept of a variable-geometry front wing for Formula Student applications.

Keywords: Formula Student aerodynamics, front wing CFD, multi-element wing, active aerodynamics, downforce.

1. Introduction

Aerodynamics plays a fundamental role in the performance of modern race cars. Even in relatively low-speed motorsport categories such as Formula Student, aerodynamic components significantly affect vehicle handling, tyre grip, and overall lap time. The primary function of aerodynamic devices is to generate downforce, which increases the normal load acting on the tyres without increasing vehicle mass [1]. Multi-element wings produce significantly higher lift coefficients compared with single-element aerofoils by exploiting increased effective camber. A CFD investigation of a Formula SAE front wing demonstrated that multi-element inverted wings generate greater downforce than single-element designs, particularly when flap angle and slot gap are optimized [2], with angle of attack identified as a primary influence on both lift coefficient and aerodynamic efficiency. Further work comparing several Formula Student front wing configurations through CFD and wind-tunnel validation confirmed that geometry optimization can yield substantial improvements in aerodynamic performance [3]. Similarly, Hokkanen [4] investigated front wing aerodynamic development for a Formula Student vehicle, providing further design benchmarks for multi-element configurations.

The front wing is the first aerodynamic component to interact with the freestream airflow, and its geometry directly influences not only the downforce it produces, but also the flow quality delivered to downstream components such as the diffuser and rear wing. When a wing operates in close proximity to the ground, the airflow beneath it accelerates due to the reduced flow area, lowering static pressure and amplifying downforce generation [5]. CFD investigations have shown that decreasing ground clearance can substantially increase aerodynamic load; however, extremely low ride heights may induce flow separation or aerodynamic stall, reducing overall efficiency.

Conventional front wings employ fixed-geometry multi-element configurations optimized for a single operating condition; however, a Formula Student vehicle must perform across a range of conditions – from tight low-speed corners requiring maximum downforce, to longer straights where drag penalizes speed. Gupta & Saxena [6] demonstrated the aerodynamic performance characteristics of a Formula SAE vehicle, establishing foundational benchmarks for downforce and drag analysis. Numerical studies of Formula Student vehicles using CFD have confirmed that aerodynamic wings significantly increase downforce while simultaneously increasing drag; despite this penalty, the additional downforce improves tyre grip and vehicle stability during cornering [7]. This trade-off motivates the investigation of a variable-geometry front wing concept in which flap incidence can be adjusted between a high-downforce closed position and a low-drag open position [8].

CFD has become a key tool for aerodynamic development in motorsport, enabling detailed flow analysis across a wide range of configurations. The objective of the present study is therefore to investigate the aerodynamic characteristics of such a variable-geometry wing using CFD methods, combining two-dimensional aerofoil analysis with full three-dimensional wing simulation. The analysis focuses on aerodynamic force coefficients, pressure distributions, and flow structures as a function of flap configuration.

1.1. Governing aerodynamic equations

The aerodynamic lift force L and drag force D acting on a body are non-dimensionalised using the dynamic pressure q and the reference planform area A to yield the lift and drag aerodynamic force coefficients:

$$C_L = L/(q \cdot A),\ C_D = D/(q \cdot A) \tag{1}$$

where L – lift force acting perpendicular to the freestream direction, N;
D – drag force acting parallel to the freestream direction, N;
A – reference planform area, m^2.

The dynamic pressure of the freestream flow is defined as:

$$q = ½\rho V^2 \tag{2}$$

where ρ – the air density, $kg \cdot m^{-3}$;
V – the freestream velocity, $m \cdot s^{-1}$.

The Reynolds number describes the ratio of inertial to viscous forces:

$$Re = \rho V c/\mu \tag{3}$$

where c – the chord length and μ is the dynamic viscosity of air.

For the present study at $V = 17\ m \cdot s^{-1}$ and $c = 0.26$ m: $Re = (1.225 \times 17 \times 0.26)/(1.812 \times 10^{-5}) \approx 2.99 \times 10^5$, confirming turbulent flow conditions appropriate for the selected turbulence model. The local pressure coefficient is defined as:

$$C_p = (p - p_\infty)/q \tag{4}$$

where negative values indicate suction regions that contribute to downforce.

2. Materials and methods

2.1. Geometry description

The three-dimensional model represents an inverted multi-element front wing based on the A18 aerofoil profile. The wing geometry was designed entirely by the authors using SolidWorks software and does not reproduce any previously published or commercially available design. The A18 aerofoil profile was used as the aerodynamic cross-section, with all spanwise dimensions, flap configurations, endplate geometry, and mounting bracket arrangements being original contributions of this study.

The geometry consists of a central mainplane element at 4° angle of attack and two outboard elements at 6°, each with a chord length of 260 mm. Two downstream flap elements (chord 160 mm) are attached to each outboard section. Two configurations are studied: (i) closed flap – flap incidence 20°, and (ii) open flap – flap elements normal to the mainplane chord, eliminating effective camber increase. Endplates at the lateral boundaries control tip vortex formation. A simplified cylindrical wheel and mounting brackets are retained in both models to capture aerodynamic interference effects (Fig. 1-3).

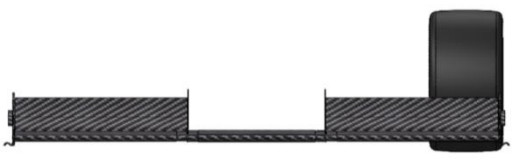

Fig. 1. **Front view of the closed-flap front wing**

Fig. 2. **Front view of the opened-flap front wing**

Fig. 3. **Left view of the opened-flap front wing**

2.2. CFD methodology – 2D analysis

Steady-state two-dimensional simulations of the aerofoil cross-section were performed in ANSYS Fluent 2025 R2 using the RANS approach with the SST k-ω turbulence model, selected for its performance in adverse pressure gradient flows and flow separation prediction [9]. Freestream conditions: $V = 17$ m·s^{-1}, $\rho = 1.225$ kg·m^{-3}, $p_\infty = 101325$ Pa, $T = 293.2$ K. Second-order upwind discretization was applied. Convergence was assessed by monitoring residuals until all fell below 1×10^{-4}.

A freestream velocity of 17 m·s^{-1} (61.2 km·h^{-1}) was selected to represent a conservative but realistic Formula Student operating condition. According to Formula Student regulations, the maximum permitted length of a single straight section is 77 m, along which vehicles typically reach speeds in the range of 60-100 km·h^{-1} depending on powertrain configuration. The lower bound of this range was adopted to ensure the results are applicable to combustion-engine vehicles, which exhibit significantly lower acceleration compared with electric competitors. Simulating at the lower end of the speed range also represents a more demanding aerodynamic condition for downforce-generating surfaces, as aerodynamic forces scale with V^2, meaning any configuration that performs adequately at 17 m·s^{-1} will generate proportionally greater downforce at higher speeds.

2.3. CFD methodology – 3D analysis

Three-dimensional simulations of the complete wing assembly were conducted in SolidWorks Flow Simulation using the RANS *k-ε* turbulence model. The computational domain extended 5 m downstream, 1.5 m upstream, 3 m above and below, and 3 m laterally, ensuring sufficient clearance to avoid boundary interference. Inlet velocity: 17 m·s^{-1}; outlet: static pressure 101 325 Pa; remaining domain faces: ideal-wall (slip) condition. Local mesh refinement was applied to all aerodynamic surfaces (Fig. 4 and 5).

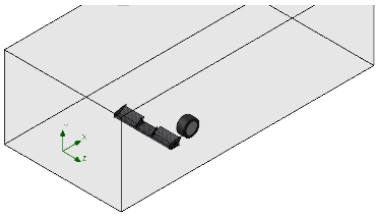

Fig. 4. **Enclosure boundary box for CFD simulation setup**

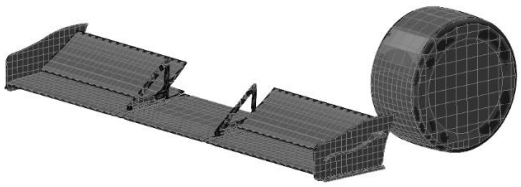

Fig. 5. **Local mesh refinement to all aerodynamic surfaces**

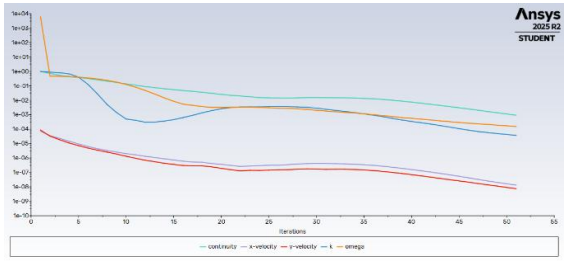

Fig. 6. **Convergence plot of closed-flap configuration**

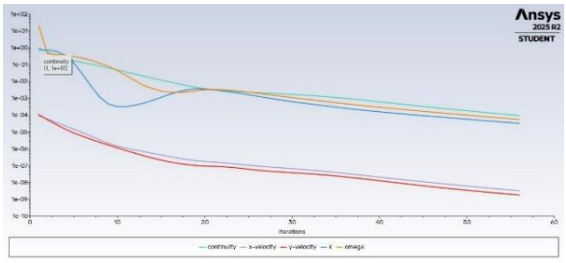

Fig. 7. **Convergence plot of open-flap configuration**

The closed-flap case converged in 303 iterations; the open-flap case in 126 iterations (Fig. 6 and 7 respectively). The open-flap case converges faster because the flow is simpler; no high-incidence separated flow at the flap, less complex wake, so the solver reaches a stable solution more quickly.

Two-dimensional simulations were performed in ANSYS Fluent, which offers precise boundary layer control and well-validated turbulence model implementations for aerofoil analysis at the mesh densities required for accurate 2D results. Three-dimensional simulations of the full wing assembly were conducted in SolidWorks Flow Simulation, which is better suited to handling the complex multi-body geometry – including mounting brackets, endplates, and wheel – within the available computational resources. This two-solver approach is consistent with established practice in academic aerodynamic studies, where 2D aerofoil analysis and 3D full-assembly simulation serve complementary but distinct roles.

3. Results and discussion

3.1. Two-dimensional aerofoil analysis

Fig. 8 and 9 show the velocity magnitude contours for both 2D configurations.

In the closed-flap case, the flow accelerates markedly on the lower (suction) surface, reaching a local maximum of approximately 28.5 m·s^{-1} – 68% above freestream – in the region between the mainplane trailing edge and the flap leading edge. This strong acceleration arises from the increased effective camber imposed by the 20° flap, which forces streamlines into a tightly curved path. The slot gap between mainplane and flap acts as a converging nozzle, directing a high-momentum jet over the upper surface of the flap to re-energise the boundary layer and delay separation. The wake downstream of the trailing edge shows a pronounced velocity deficit consistent with the higher drag of this configuration.

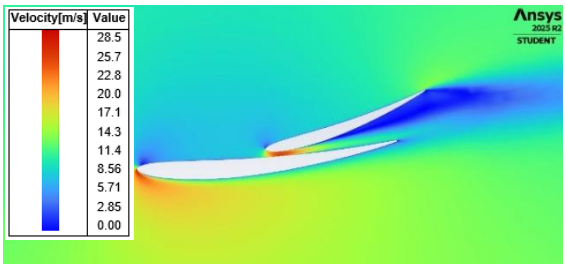

Fig. 8. **Velocity magnitude of closed-flap, 2D analysis**

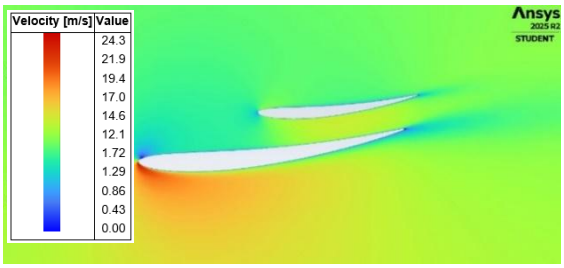

Fig. 9. **Velocity magnitude of open-flap, 2D analysis**

In the open-flap configuration, peak velocity is reduced to approximately 24.3 m·s^{-1}, reflecting the lower effective camber. The wake is noticeably thinner, consistent with the 60.5% reduction in the drag coefficient.

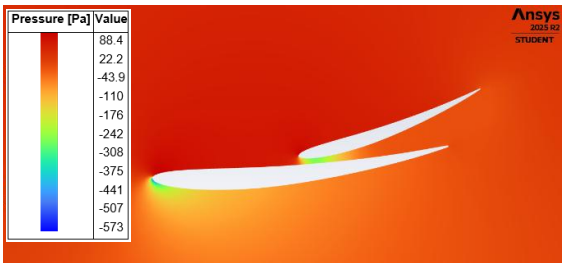

Fig. 10. **Pressure contour of closed-flap, 2D analysis**

Fig. 11. **Pressure contour of open-flap, 2D analysis**

The 2D pressure contours (Fig. 10 and 11) confirm a strong suction region on the lower surface of the closed-flap configuration. The minimum gauge pressure at the flap suction surface is approximately −573 Pa, giving a pressure coefficient $C_{p,min} = -573/177.0 \approx -3.2$. This strong suction peak identifies the flap leading edge region as the primary source of downforce. The stagnation zone at the mainplane

leading edge shows gauge pressures up to + 88 Pa ($C_p \approx +0.50$). For the open-flap configuration, the minimum suction is reduced to $C_{p,min} \approx -2.22$, consistent with the lower effective camber.

Table 1 summarises the 2D aerodynamic coefficients. Despite generating 24.1% less downforce, the open flap reduces drag by 60.5% and more than doubles the aerodynamic efficiency ratio, confirming its advantage for straight-line performance.

Table 1

2D aerodynamic coefficients (ANSYS Fluent, $V = 17$ m·s^{-1})

Configuration	C_L	C_D	$\lvert C_L \rvert / C_D$
Closed flap	−0.635	0.049	12.9
Open flap	−0.482	0.019	24.7
Change	−24.1%	−60.5%	+ 91.5%

Residual convergence plots (Fig. 6 and 7) confirm numerical reliability. All residuals – continuity, x-velocity, y-velocity, k, and ω – fall below 1×10^{-4} within approximately 55 iterations, with k and ω reaching 1×10^{-8}, confirming well-resolved steady-state solutions.

3.2. Three-dimensional full wing CFD analysis

Table 2 presents the converged aerodynamic force goals from the three-dimensional simulations. The freestream dynamic pressure at 17 m·s^{-1} is $q = 177.0$ Pa. Using the reference planform area $A = 0.312$ m^2 (chord 0.26 m × span 1.2 m), the three-dimensional aerodynamic coefficients and minimum pressure coefficients are given in Table 3.

Table 2

3D CFD results summary (SolidWorks Flow Simulation, $V = 17$ m·s^{-1})

Parameter	Closed flap	Open flap	Change
Downforce, N	43.45	28.01	-35.5%
Drag force, N	19.41	10.04	-48.3%
Max velocity (X), m·s^{-1}	28.16	20.07	-28.7%
Max dynamic pressure, Pa	509.6	320.8	-37.1%
Iterations to converge	303	126	–

Table 3

3D aerodynamic coefficients and $C_{p,min}$ ($A = 0.312$ m^2, $V = 17$ m·s^{-1})

Configuration	C_L	C_D	$\lvert C_L \rvert / C_D$	$C_{p,\min}$
Closed flap	0.787	0.351	2.24	-3.2
Open flap	0.507	0.182	2.79	-1.49
Change	-35.5%	-48.3%	+ 24.6%	-53.0%

The three-dimensional lift coefficients ($C_L = 0.787$ and 0.507) are higher than their corresponding two-dimensional values ($|C_L| = 0.635$ and 0.482). This is physically consistent and expected. In the two-dimensional aerofoil analysis, no endplates are present, meaning the pressure differential between the upper and lower surfaces is free to equalise at the wing tips, generating spanwise flow and tip vortices that reduce the effective downforce contribution across the span. In the three-dimensional assembly, the endplates suppress this spanwise pressure equalization, confining the low-pressure suction region to the lower surface and allowing it to act more effectively across the full span.

This containment effect increases the net downforce generated by the wing, which is directly beneficial for cornering performance in Formula Student applications. The trade-off is a moderate increase in drag in the three-dimensional case, attributable to the additional wetted surface area of the endplates and the interference drag introduced at the endplate-mainplane junctions.

3.3. Velocity field – closed flap (3D)

The velocity flow trajectories for the closed-flap configuration (Fig. 12) reveal three-dimensional flow behaviour not captured in 2D. The freestream is deflected downward beneath the inverted mainplane, accelerated through the slot gap, and discharged at the flap trailing edge at up to 28.16 m·s^{-1}. Of particular significance is the strong upwash component: at 20° flap incidence, the trailing flow exits with substantial upward momentum and impinges directly on the adjacent tyre. This aerodynamic interaction increases the effective drag of the wheel assembly [10] and represents an important three-dimensional penalty of the closed-flap configuration.

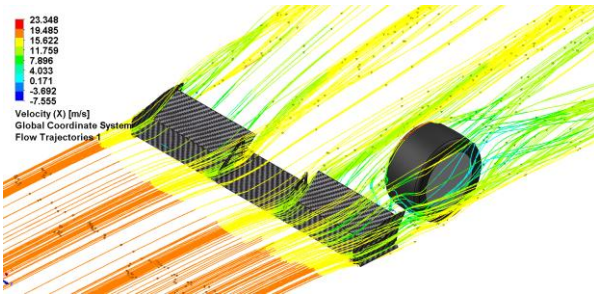

Fig. 12. **Velocity flow trajectories for closed-flap configuration**

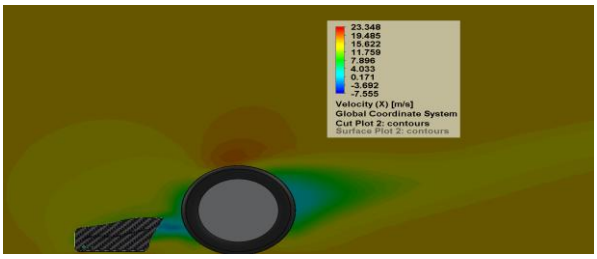

Fig. 13. **Velocity cut plot for closed-flap configuration**

The velocity cut plot (Fig. 13) shows the accelerated suction-side flow (orange, ~23 m·s^{-1}) and the extensive low-velocity wake region extending rearward past the wheel.

3.4. Pressure distribution – closed flap (3D)

The surface pressure contour (Fig. 14) confirms a pronounced suction region on the lower mainplane surface, reaching a minimum of 100,764 Pa absolute (gauge: −561 Pa, $C_{p,min} \approx -3.2$), consistent with the 2D result. Pressure distribution is uniform across the three spanwise sections, indicating consistent aerodynamic loading. The endplates maintain a pressure barrier at lateral boundaries, preserving suction on the lower surface. The pressure cut plot (Fig. 15) shows pressure concentrated at the flap surfaces and dissipating rearward-upward – characteristic of high-incidence flap operation.

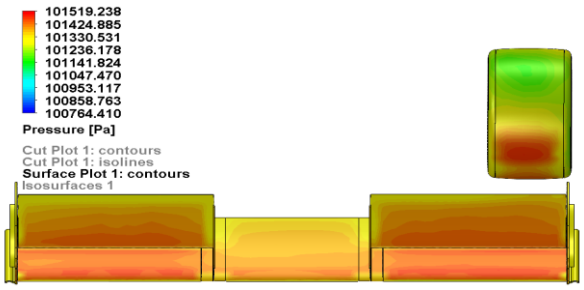

Fig. 14. **Surface pressure contour for closed-flap front wing**

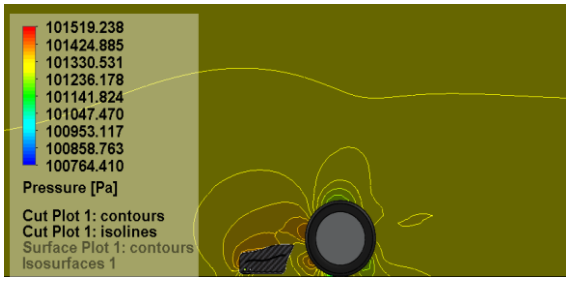

Fig. 15. **Pressure cut plot for closed-flap front wing**

3.5. Velocity field – open flap (3D)

The velocity trajectories for the open-flap configuration (Fig. 16) show a markedly different, more orderly flow. With the flap normal to the mainplane chord, air passes through the open gap with minimal deflection. The maximum local velocity is 20.07 m·s^{-1} – only marginally above freestream – confirming that the open flap does not strongly accelerate the flow. Upwash is substantially reduced: the trailing flow no longer impinges on the tyre with high upward momentum, eliminating the wheel-interaction drag penalty of the closed configuration. The velocity cut plot (Fig. 17) shows a thin, well-organised wake, consistent with the lower drag coefficient.

Fig. 16. **Velocity trajectories for open-flap case**

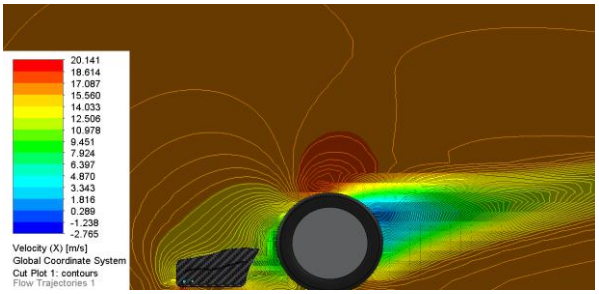

Fig. 17. **Velocity cut plot for open-flap configuration**

3.6. Pressure distribution – open flap (3D)

The surface pressure contour (Fig. 18) reveals a substantially reduced pressure differential: $C_{p,min} \approx -1.49$, compared with −3.2 in the closed configuration. This 53% reduction in suction intensity directly explains the 35.5% reduction in downforce. One notable consequence of the open configuration is that the freestream now flows more directly toward the wheel, increasing the stagnation pressure on the tyre's mid-plane – a secondary aerodynamic disadvantage that partially offsets the gains on the wing itself.

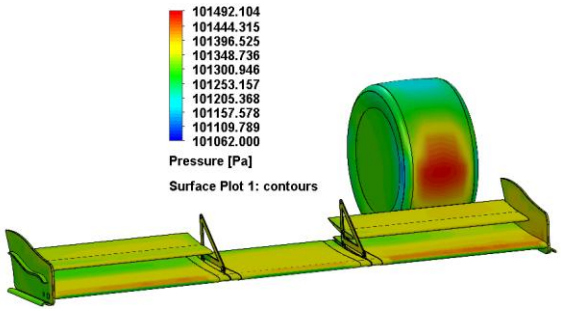

Fig. 18. **Surface pressure contour for open-flap case**

The present results are broadly consistent with findings reported in comparable Formula Student and Formula SAE aerodynamic studies. Chen [2] reported lift coefficients in the range of $|C_L| = 0.5–0.8$ for multi-element Formula SAE front wings, which aligns with the 2D values of 0.482–0.635 obtained in the present study. Krbat'a et al. [3] demonstrated that flap angle optimisation can yield significant performance differences between configurations, consistent with the 24.1% downforce reduction observed here when switching from the closed to the open configuration. Hokkanen [4] similarly reported that endplate geometry substantially influences spanwise pressure distribution, in agreement with the present finding that 3D lift coefficients exceed their 2D counterparts due to endplate containment effects. The drag coefficients obtained in the present 3D simulation ($C_D = 0.182$-0.351) are somewhat higher than those reported by Gupta and Saxena [6] for simpler single-element configurations, which is expected given the additional wetted area of the multi-element design. Noor et al. [7] confirmed that downforce improvements from front wing additions come at the cost of increased drag, a trade-off quantified in detail in the present study. Overall, the present results fall within the range reported in the literature and reinforce the established understanding of multi-element front wing aerodynamics in Formula Student applications.

4. Limitations and Scope

The present simulations model the front wing assembly in isolation, including simplified wheel geometry and mounting brackets, but excluding the vehicle chassis, driver, sidepods, rear wing, and underbody. The addition of these components would be expected to influence the results in several ways. The chassis and driver geometry would introduce a large upstream blockage effect, modifying the pressure field approaching the front wing and reducing the effective freestream velocity seen by the wing. The underbody and diffuser would alter the overall pressure balance of the car, potentially

reducing the relative contribution of the front wing to total downforce. The rear wing would generate its own wake, which at the velocities considered would not directly affect the front wing but would change the overall aerodynamic balance of the vehicle. Furthermore, the interaction between the front wing wake and downstream components – particularly the sidepods and radiator inlets – would introduce additional drag not captured in the present model. As a result, the absolute values of C_L and C_D reported here are expected to be higher than those that would be obtained from a full-car simulation, where aerodynamic interference between components typically reduces the net efficiency of individual elements. Nevertheless, the relative trends between the closed-flap and open-flap configurations are expected to remain valid, as both configurations were simulated under identical domain and boundary conditions.

Conclusions

1. Two-dimensional CFD analysis yields $C_L = -0.635$, $C_D = 0.049$ for the closed-flap and $C_L = -0.482$, $C_D = 0.019$ for the open-flap configuration, representing a 24.1% reduction in downforce and 60.5% reduction in drag when the flap is opened.
2. Three-dimensional simulations confirm this trend at full wing scale: downforce reduces from 43.5 N to 28.0 N (−35.5) and drag from 19.4 N to 10.0 N (−48.3%) when switching to the open-flap configuration.
3. Pressure analysis identifies suction peaks of $C_{p,min} \approx -3.2$ at the flap leading edge in the closed configuration, confirming this region as the primary source of downforce generation in both 2D and 3D.
4. Three-dimensional flow trajectory analysis reveals that the 20° closed flap generates significant upwash that directly impinges on the adjacent wheel, creating additional aerodynamic drag – a three-dimensional effect absent in 2D analysis that highlights the importance of full-assembly simulation.
5. The open-flap configuration improves aerodynamic efficiency ($|C_L|/C_D$) by 24.6% in three dimensions, supporting its use as a straight-line performance mode. The closed configuration remains preferable for cornering, where maximum downforce and tyre grip are required.
6. The results demonstrate the aerodynamic viability of a variable-geometry front wing concept, providing a quantitative basis for further development of adaptive aerodynamic systems in future Formula Student frameworks.

The aerodynamic efficiency ratio $|C_L|/C_D$ is a key metric for aerodynamic performance assessment. A lower drag coefficient C_D reduces aerodynamic resistance and improves straight-line speed, while a higher $|C_L|$ increases the normal load on the tyres, improving cornering grip and vehicle stability. In general, a higher $|C_L|/C_D$ ratio indicates better overall aerodynamic efficiency, meaning the wing generates more downforce per unit of drag penalty. This ratio is therefore critical for Formula Student applications, where the trade-off between downforce and drag directly governs laptime performance across different track sections.

Acknowledgements

The authors would like to express their sincere gratitude to the Vice-Dean of the Faculty of Civil Engineering and Mechanical Engineering of RTU and the Director of the Institute of Mechanical and Biomedical Engineering of RTU, Ivo Vaicis, for the support and funding of the project.

Author contributions

Conceptualization, A.A., N.K.; methodology, A.A., N.K. and S.S.; software, A.A. and N.K.; validation, A.A., N.K. and S.S.; formal analysis, A.A., N.K.; investigation, A.A. and N.K.; data curation, A.A.; writing – original draft preparation, A.A.; writing – review and editing, S.S.; visualization, A.A. and N.K.; project administration, S.S. All authors have read and agreed to the published version of the manuscript.

References

[1] Katz J. Aerodynamics of race cars. Annual Review of Fluid Mechanics, 38, 2006, pp. 27-63. DOI: 10.1146/annurev.fluid.38.050304.092016

[2] Chen X. Analysis and improvements of a front wing for formula SAE car. Theoretical and Natural Science, 13, 2023, pp. 136-143. DOI: 10.54254/2753-8818/13/20240822
[3] Krbaťa M., Fekič J. J., Kohutiar M., Malý M., Mikuš P. Design and optimization of the front wing for formula student monopost. In Advances in Science and Technology, Vol. 167, 2025, pp. 3-13. DOI: 10.4028/p-o8TWSo
[4] Hokkanen M. Aerodynamic development of a formula student front wing [Bachelor's thesis, KTH Royal Institute of Technology]. DiVA, 2024. [online] [11.02.2026] Available at: https://www.diva-portal.org/smash/get/diva2:1881327/FULLTEXT01.pdf
[5] Soso M. D., Wilson P. A. Aerodynamics of a wing in ground effect in generic racing car wake flows. Proceedings of the Institution of Mechanical Engineers, Part D: Journal of Automobile Engineering, 220(1), 2006, pp. 1-13. [online] [11.02.2026] Available at: https://www.researchgate.net/publication/238186393_Aerodynamics_of_a_wing_in_ground_effect_in_generic_racing_car_wake_flows
[6] Gupta S., Saxena K. Aerodynamics analysis of a formula SAE car. In Proceedings of the 13th International Conference on Heat Transfer, Fluid Mechanics and Thermodynamics, 2017. [online] [11.02.2026] Available at: https://repository.up.ac.za/bitstream/handle/2263/62356/Gupta_Aerodynamics_2017.pdf
[7] Noor D. Z., Mirmanto H., Anzip A., Sasongko H. Influence of front and rear wings on aerodynamic forces in a student formula car. The International Journal of Mechanical Engineering and Sciences, 8(2), 2024, pp. 76-83. [online] [11.02.2026] Available at: https://iptek.its.ac.id/index.php/jmes/article/view/21073
[8] Broniszewski J., Piechna J. A fully coupled analysis of unsteady aerodynamics impact on vehicle dynamics during braking with an active front wing. Engineering Applications of Computational Fluid Mechanics,13(1), 2019, pp. 677-695. [online] [11.02.2026] Available at: https://www.researchgate.net/publication/334368577_A_fully_coupled_analysis_of_unsteady_aerodynamics_impact_on_vehicle_dynamics_during_braking
[9] Menter F. R. Two-equation eddy-viscosity turbulence models for engineering applications. AIAA Journal, 32(8), 1994, pp. 1598-1605. DOI: 10.2514/3.12149
[10] Diasinos S., Barber T. J., Doig G. The effects of simplifications on isolated wheel aerodynamics. Journal of Wind Engineering and Industrial Aerodynamics, 146, 2015, pp. 90-101. DOI: 10.1016/j.jweia.2015.08.004